



Supporting Online Material for

Atmospheric Warming and the Amplification of Precipitation Extremes

Richard P. Allan* and Brian J. Soden

*To whom correspondence should be addressed. E-mail: r.p.allan@reading.ac.uk

Published 7 August 2008 on *Science Express*

DOI: 10.1126/science.1160787

This PDF file includes:

Materials and Methods

SOM Text

Figs. S1 to S7

Table S1

References

Supporting Online Material

1. Materials and Methods

a. SSM/I data

Precipitation estimates from SSM/I are available over the oceans twice-daily as ascending and descending orbital overpasses from Remote Sensing Systems (RSS; <http://www.ssmi.com>) at a horizontal resolution of 0.25×0.25 degrees (S1). For comparison with coarser climate model grids, this resolution was degraded to 2.5×2.5 degrees. Daily data were constructed by averaging the ascending and descending overpasses. We considered the satellites F08 (July 1987 to December 1991), F11 (January 1992 to April 1994) and F13 (May 1995 to December 2003) since inter-calibration is judged to be superior to the remaining satellites in the series, based on time series of tropical ocean mean precipitation.

Considering grid-points of non-zero precipitation over the tropical oceans (30°S - 30°N), percentile bins of precipitation rate were calculated, ranging from the lightest 10% to the heaviest 10%. Ten decile bins (0-10%, 10-20%, ...90-100%) were considered; in addition, the heaviest 10% of daily rainfall events were further partitioned into the 90-95%, 95-99% and 99-100% bins, making a total of 12 bins. The bin boundaries were calculated using the first year of daily SSM/I data (July 1987-June 1988) at the 0.25° and 2.5° resolutions; using different years and satellites to set the bin boundaries made only small differences (Table S1). Using instantaneous (ascending and descending) data increases the precipitation rates used at the bin boundaries while averaging over more than one days data reduces the precipitation rate at the boundaries as expected. For the purposes of the model comparisons we use daily averages (ascending plus descending) unless stated (highlighted as bold in Table S1).

b. Model data

Daily precipitation was taken from the Program for Climate Model Diagnosis and Intercomparison (PCMDI; <http://www-pcmdi.llnl.gov>) CMIP3 climate model archive (S2). The model simulations were atmosphere only experiments forced with observed sea surface temperature (SST) and fixed present day greenhouse gas and aerosol concentrations, although the CNRM simulation included prescribed greenhouse gas increases while the GISS model included volcanic aerosol forcing. Precipitating grid-points were used to construct precipitation bin boundaries, as for the SSM/I data, using daily values for 1985. Using different years made little impact on the bin boundaries, for example shown for the GISS_E_R model (Table S1). Where $P < 1 \times 10^{-6} \text{ mm/day}$, precipitation was assumed to be zero. Replacing this with the minimum daily SSM/I precipitation of 0.08 mm/day did not impact the results substantially (Section 2b).

The calculated model precipitation percentile bin boundaries are documented in Table S1. There is a large spread in values depending upon the model used. In particular the GISS model, which is low resolution compared to many of the models, produces substantially larger precipitation rates for the bin boundaries. Regridding the models to the 2.5×2.5 degree resolution tends to reduce the range of precipitation intensities (Table S1) but does not impact noticeably the variability in precipitation frequency in each bin. Nevertheless lower resolution models will be less able to represent the processes involved in resolving accurately heavy rainfall events.

The SSM/I bin boundaries are also generally larger than the model data, reflecting the fact that models struggle to simulate the present day probability distribution of precipitation intensity (S3). As such, the variability will sample smaller precipitation rates in the models and this should be considered in the comparisons between models and satellite data. For example, the 60th percentile for the SSM/I 2.5×2.5 degree daily data for 1987/88, of around 6 mm/day , corresponds most closely with the 80th percentiles for most models. These differences also reflect the different sampling between the satellite data, which sample instantaneous fields, and the models which are true daily averages. Nevertheless, since the changes in frequency of events in each percentile are computed, the lightest and heaviest rainfall events are being sampled regardless of the differences in actual precipitation rate. This is confirmed by the consistency in percentage changes in frequency of precipitation in each bin using differing averaging periods (Section 2b).

c. Method

To calculate the frequency of precipitation occupying each bin, the following method was applied to the model and satellite data. For each month (m) of each year (y), daily tropical ocean precipitation fields were obtained and the fraction of precipitating grid-points, $f(P)_{[y,m,b]}$, falling within each percentile bin (b) was calculated. This strategy was adopted to account for the inconsistencies between model and observed precipitation distributions (S3) such that the lightest or heaviest 10% of precipitation events, for example, were given equal weight in the models and satellite data. Variability of the fraction of oceanic precipitating grid points is small for the models and satellite data (less than 2% standard deviation). The difference in frequency was taken relative to the mean frequency for that month $\overline{f(P)_{[m,b]}}$, thereby removing any seasonal signal, and this was normalized by the overall mean frequency for each bin $\overline{f(P)_b}$ such that a percentage frequency anomaly was calculated as a function of time and bin:

$$P\%_{[y,m,b]} = 100(f(P)_{[y,m,b]} - \overline{f(P)_{[m,b]}}) / \overline{f(P)_b}. \quad (1)$$

The normalization ensures that, for example, the mean frequency of the 0-10% bin is 0.1 and for the 99-100% bin it is 0.01. Without this normalization the mean frequencies deviate slightly from these values due to the discretization of the data. For example, using the GFDL model output, the mean frequency deviates from its percentile bin width by less than 6%. Since percentage anomalies of the normalized frequencies are taken, equal weight is given to the variability in each bin. While the spatial distribution of precipitation contributes to the precipitation frequency in each bin, here we are concentrating on the temporal variability in the frequency distribution and its relationship with SST.

For the satellite data, frequency anomalies are taken with respect to the means for the particular satellite used for each month. The F08, F11 and F13 satellites exhibit much closer correspondence in mean precipitation than the remaining satellites in the series and the results are not sensitive

to this choice (Section 2b). Nevertheless, calculating frequency anomalies separately for each satellite ensures that small discontinuities between satellites are removed and the response to interannual variability is captured.

The calculated variability in precipitation frequency is presented in Figure S1 for the SSM/I data at 0.25° (F08 and F13 only) and 2.5° resolution for the ten decile bins of precipitation. A consistent picture is evident in the heaviest rainfall decile bin with more frequent rainfall in this bin during warm El Niño months (e.g., 1997/98) and a lower occurrence in cold La Niña months (e.g., 1999-2000). There is greater coherence in the variability for the high resolution satellite data although the lowest two bins appear saturated with respect to discretisation of the data. While it would be interesting to compare the high resolution data with high resolution model output in the future, for comparison with current climate models it is more informative to compare the degraded satellite data resolution with the model data since they are more comparable in resolution.

2. Supporting Online Material: Text

a. *Precipitation frequency variability*

Figure S2 shows the fluctuations in precipitation frequency for each model. This demonstrates that all model simulations produce coherent responses to the warming and cooling over the El Niño Southern Oscillation (ENSO) cycle. The MIROC models appear to produce a smaller percentage precipitation response than the other models and also contain the fewest number of non-precipitating grid-points. Improved agreement between the model ensemble mean variations and the satellite data is attained for the heaviest rainfall bins when only the 20% wettest model grid boxes are sampled (Fig. S3). Essentially, in this case, model precipitation is set to zero in the 80% of driest of all grid boxes, masking out the large quantity of light rainfall simulated by the models (S3). Variability of precipitation frequency is quantified in Figure S4 by calculating the standard deviation for each bin. The variability is consistent between the model ensemble mean and the satellite data (within 3%) but is generally smaller than for individual models.

b. *Sensitivity of Precipitation Frequency to SST*

The sensitivity of precipitation frequency in each bin to changes in SST is presented in Figure S5 for different processing strategies. Fig. S5a shows the SSM/I frequency anomalies with respect to the entire satellite record (red line) in addition to the standard approach of treating each satellite separately (black line). Also shown are sensitivities calculated using instantaneous SSM/I data (light blue), using two-day averaging (dark blue) and calculating sensitivities for a shorter time period (1988-2000, dotted line). The overall pattern of reduced occurrence of light and moderate precipitation and increased occurrence of heavy precipitation is reproduced and sensitivities are within 5 %/K for all but the 99-100% bin for the 2-day averaging which produces a sensitivity 8 %/K lower than the standard approach.

For the daily average SSM/I product, the minimum precipitation observed, determined by the instrument sensitivity, is 0.08 *mm/day*. This is substantially larger than the instantaneous 0.25×0.25 degree product due to averaging but relevant to the coarse climate model grids. This threshold may impact the comparisons with the model simulations since light rainfall below this threshold is included in the analysis. However, when all rainfall below 0.08 *mm/day* is set to zero in the models, the resulting sensitivity is within 5%/K of the standard calculations (Fig. S5b, red line). A closer match to the observational sensitivity distribution with precipitation intensity bin is attained where only the 20% wettest of all model grid boxes over the tropical ocean are sampled (gray line). In this case, the lightest model rainfall is essentially masked from the analysis by ensuring that 80% of the driest of all model grid boxes (precipitating and non-precipitation) are reset to zero precipitation. This may relate to the overprediction of light rainfall by models compared to the satellite data (S3).

The sensitivity of precipitation frequency to SST where one year (1985) of daily precipitation fields from the GFDL model are scaled by 7% times the local SST anomaly (Clausius Clapeyron experiment) is shown in Figure S6a. Also shown is the simple case where the same year of daily precipitation fields are increased by 7% (diamonds), effectively assuming a uniform 1 K warming and 7 %/K precipitation response. The reduction in frequency of light precipitation and increased frequency of very heavy precipitation is expected in this case since the probability distribution of precipitation is constrained to shift to higher percentile bins with increased SST. Divergence of the

Clausius Clapeyron experiment from this response would require local SST changes associated with the heaviest or lightest bins to be anti-correlated with the mean SST response. This does not appear to be the case since the linear fit (red line) and El Niño minus La Niña case (light blue line) reproduce the simple response apart from in the heaviest bin where the linear fit underestimates the response and the El Niño minus La Niña response produces a negative response. The model ensemble mean displays anti-correlation with the Clausius Clapeyron experiment in the lightest rainfall bin, instead showing an increase in the frequency of light rainfall with increased SST.

The sensitivity of precipitation frequency to anthropogenically forced climate change is presented in Figure S6b. The changes in precipitation frequency in response to the tropical ocean warming from 2001-2005 to 2101-2105 ($2.2 K$) show similarity to the response expected from Clausius Clapeyron for the present climate (Fig. S6a) although the response of the heaviest precipitation is lower than the linear fit. The Clausius Clapeyron response is also calculated using the 2101-2105 minus 2001-2005 SST difference pattern to drive increases in precipitation at $7\%/K$ (red line), expected from Clausius Clapeyron, and $3\%/K$ (black line), closer to the mean precipitation response found in climate change projections (S4). These responses are larger than the climate change simulated response for the heaviest rainfall bins. One reason for the discrepancy is that greenhouse gas increases exert a heating effect on the atmosphere which, assuming small changes in sensible heat transfer, require reduced latent heating of the atmosphere through precipitation to balance (S5).

To examine the impact of this process, we estimate the forcing over the period 2000-2100 to be around $4.5 Wm^{-2}$ (S6). Assuming that one third of this heats the surface directly and the remainder heats the atmosphere (S5, S7) this translates to around a $3 Wm^{-2}$ heating of the atmosphere. Assuming this extra radiative heating is balanced by reduced latent heating through precipitation, this would require a $0.1 mm/day$ reduction in precipitation, around 3% of the global mean, consistent with previous estimates (S5). Therefore we conduct a final experiment in which daily precipitation fields for the 2101-2105 period are scaled by -3% and the differences in the precipitation frequency distribution are replotted in Fig. S6b (triangles). This more closely matches, although is marginally lower than, the $3\%/K$ response for the heaviest precipitation bins.

c. Water vapor content by precipitation bin

In explaining the co-variability of precipitation and tropical ocean warming, the rises in column integrated water vapor (CWV) are crucial (S1,S8). Unfortunately the model archive does not include daily CWV. However, there is a clear rise in daily CWV with increasing daily precipitation in the SSM/I data; CWV rises at approximately $1.7mm$ for each 10% bin of precipitation, from $39mm$ in the 0-10% bin up to $55mm$ for the 99-100% bin (Fig. S7). The observed El Niño minus La Niña warming is $0.12 K$ is accompanied by increased CWV of around 1% , a rate of about $8\%/K$ for all bins as expected from the Clausius Clapeyron relationship (S1). While moisture rises with SST in all bins, it is only in the heaviest rainfall bins, where rainfall occurs primarily by moisture convergence (S8), that substantial rises in precipitation frequency are observed.

3. Supporting Online Material: Figures

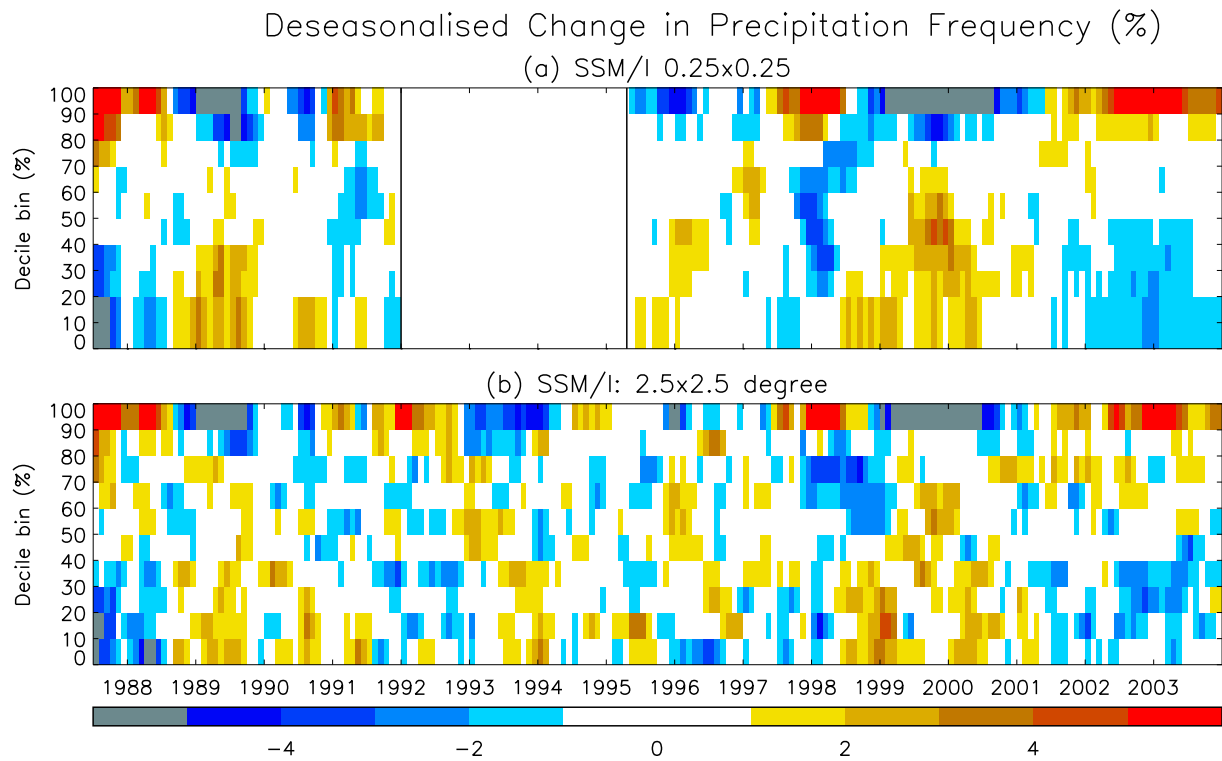


FIG. S 1. Histograms of percentage changes in precipitation frequency in decile bins for the SSM/I data for (a) 0.25×0.25 degree and (b) 2.5×2.5 degree resolutions

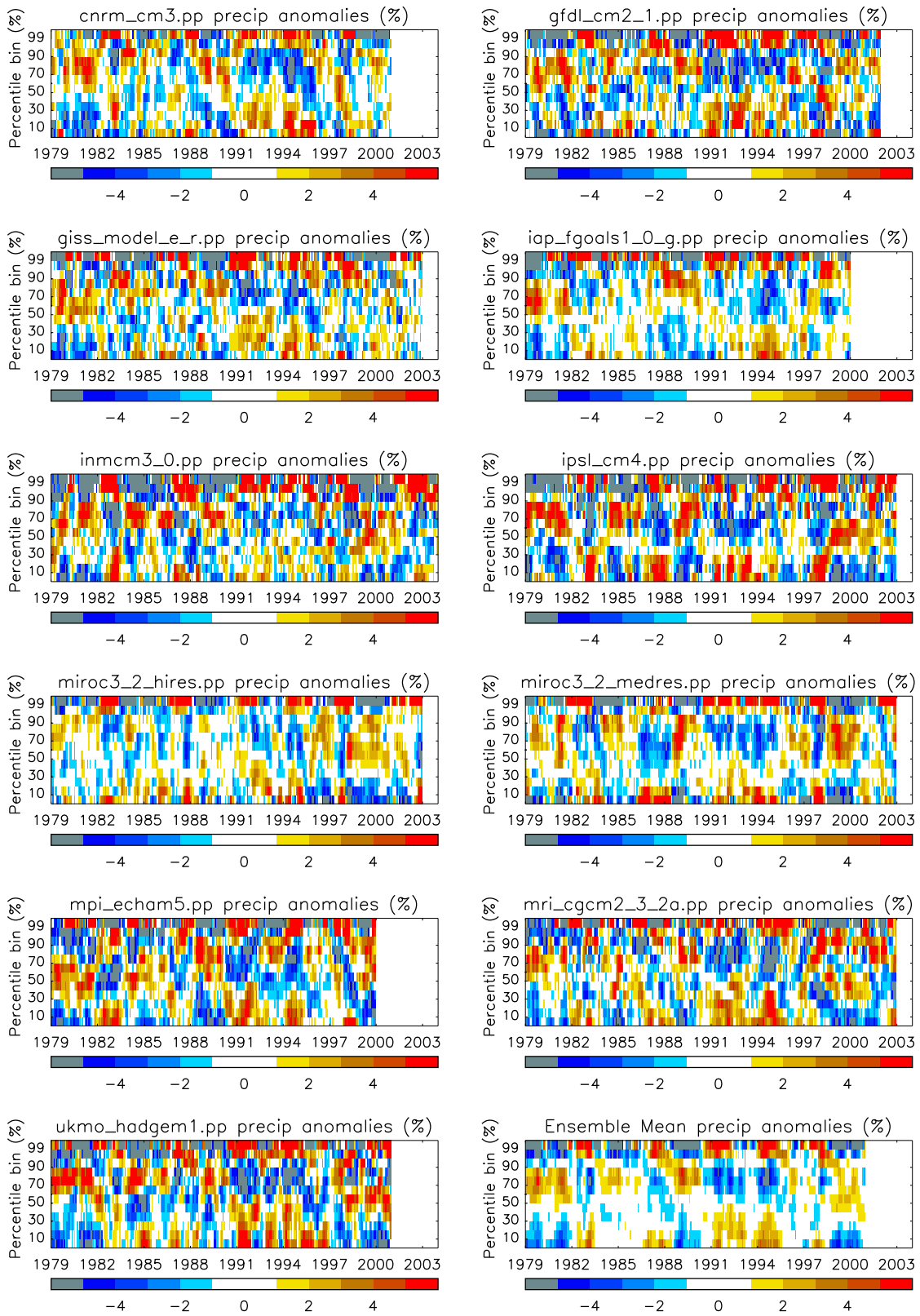


FIG. S 2. Histograms of percentage anomalies in frequency of precipitation in percentile bins of precipitation for 11 climate models

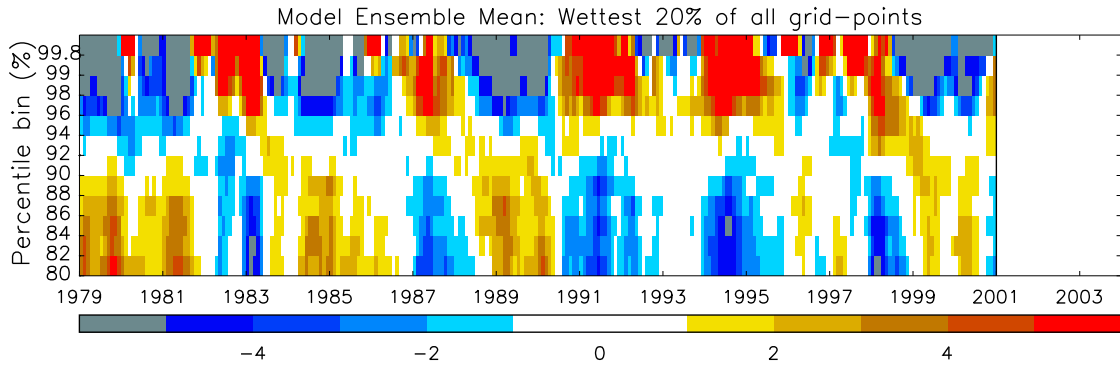


FIG. S 3. Histograms of percentage anomalies in frequency of precipitation in percentile bins of precipitation for climate models ensemble mean when considering only the 20% wettest of all grid-boxes (or ensuring that 80% of the driest of all model grid-boxes are non-precipitating).

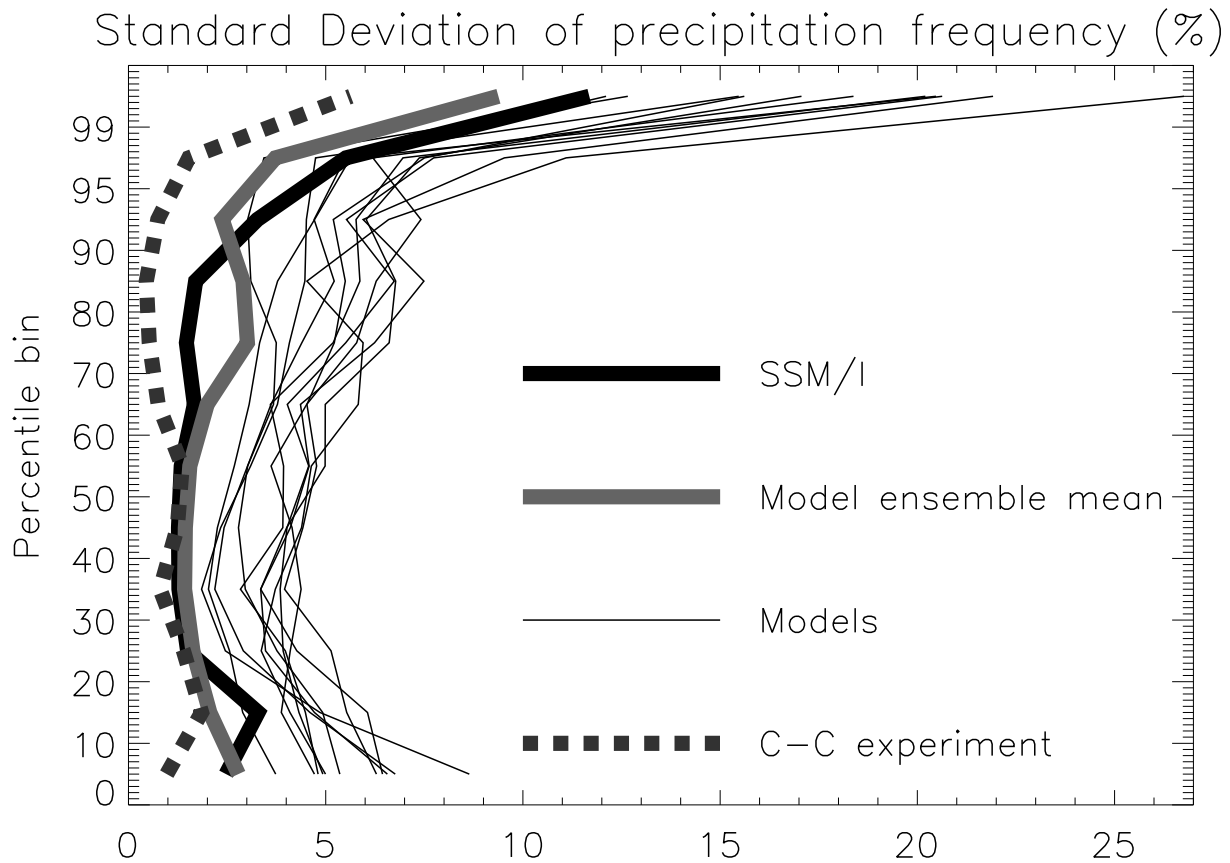


FIG. S 4. Standard Deviation of percentage variability in the frequency of occurrence of precipitation for bins of precipitation intensity for SSM/I, models, model ensemble mean and the Clausius Clapeyron experiment

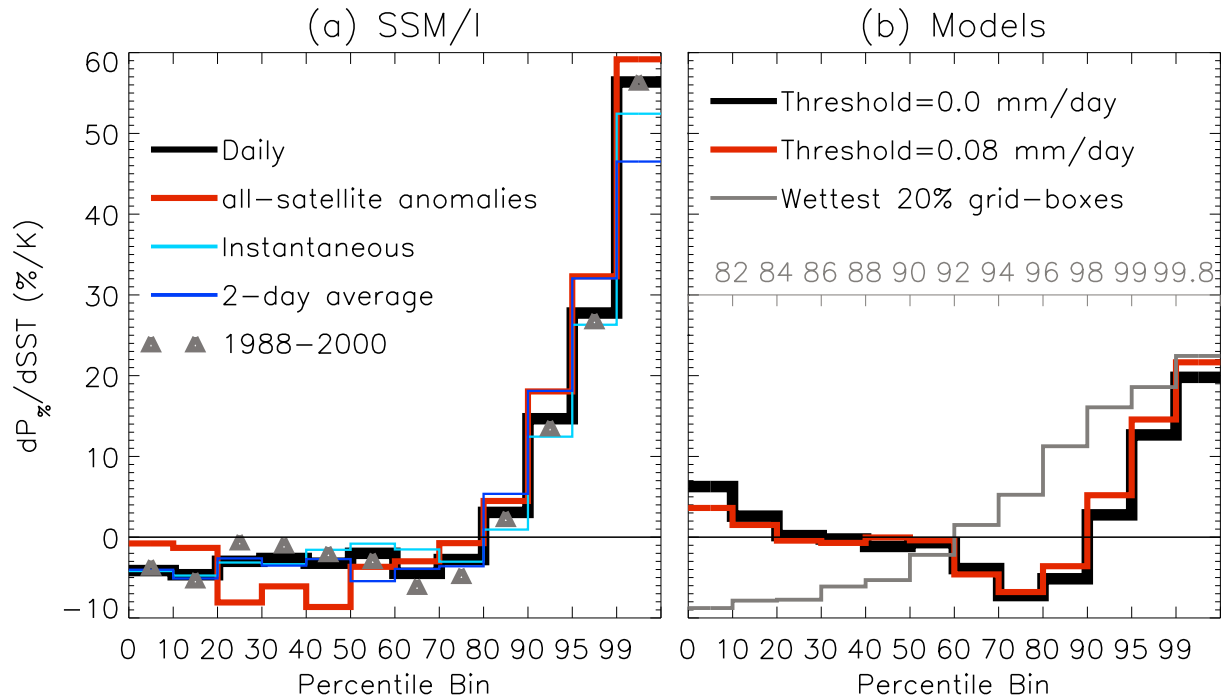


FIG. S 5. Sensitivity of precipitation frequency to changes in SST for the (a) SSM/I data using different methods of processing the data and (b) the model ensemble mean for different thresholds below which precipitation is assumed to be zero. In b the 20% wettest grid boxes case essentially sets 80% of the driest of all model grid boxes over the tropical oceans to zero precipitation.

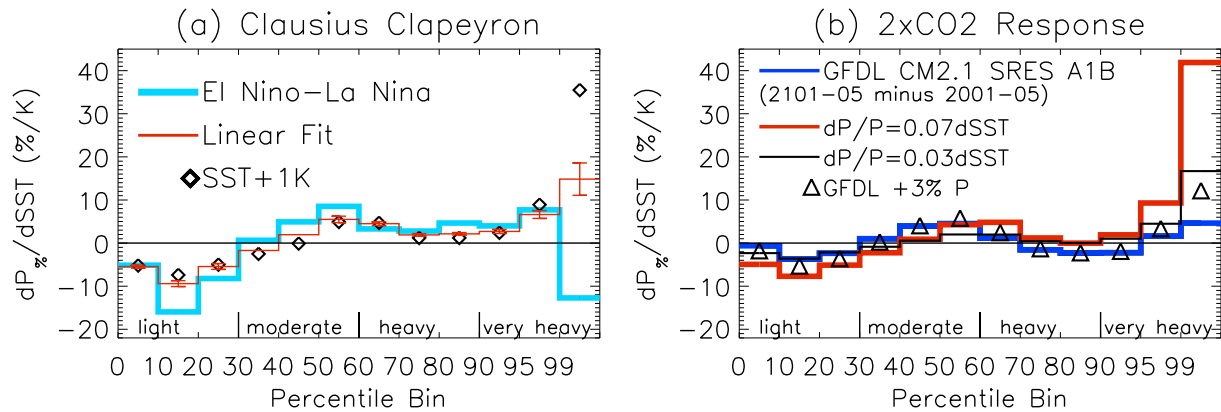


FIG. S 6. Sensitivity of precipitation frequency to changes in SST for (a) Clausius Clapeyron experiments and (b) the GFDL scenario A1B climate prediction experiment.

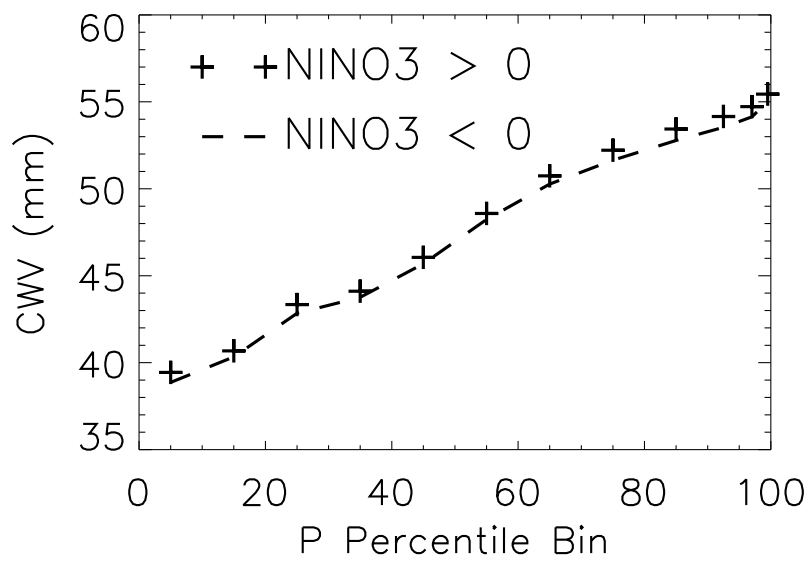


FIG. S 7. Mean daily column integrated water vapor (CWV) in bins of precipitation intensity for El Niño (NINO3 > 0) and La Niña (NINO 3 < 0) months

4. Supporting Online Material: Table

TABLE S 1. Precipitation bin boundaries (mm/day) calculated for various space and time resolutions and years for the SSM/I data and for each individual model

Data	Resolution	Year	Bin (%)										
			10	20	30	40	50	60	70	80	90	95	99
SSM/I	$0.25^\circ \times 0.25^\circ$	1987/88	0.24	0.46	0.89	1.73	3.6	7.92	15.8	29.8	61.0		
SSM/I	$2.5^\circ \times 2.5^\circ$	1987/88	0.22	0.46	0.89	1.61	3.6	7.44	15.1	29.0	60.0	102.9	252.0
SSM/I	$2.5^\circ \times 2.5^\circ$	1990	0.22	0.46	0.84	1.51	3.1	6.7	13.9	27.1	55.9		
SSM/I	$2.5^\circ \times 2.5^\circ$	1988	0.22	0.46	0.89	1.56	3.4	7.0	14.4	27.6	57.6		
SSM/I daily	$2.5^\circ \times 2.5^\circ$	1987/88	0.22	0.36	0.67	1.27	2.9	6.2	12.5	24.0	49.9	84.7	206.4
SSM/I daily	$2.5^\circ \times 2.5^\circ$	1992	0.22	0.38	0.67	1.34	2.88	6.26	12.7	24.4	51.1	89.6	222.3
SSM/I daily	$2.5^\circ \times 2.5^\circ$	1995/96	0.22	0.33	0.67	1.25	2.85	6.25	12.7	23.7	49.3	84.5	205.9
SSM/I 2 days	$2.5^\circ \times 2.5^\circ$	1987/88	0.12	0.22	0.46	0.89	2.1	4.6	8.9	17.3	35.5	60.0	139.2
SSM/I 3 days	$2.5^\circ \times 2.5^\circ$	1987/88	0.089	0.18	0.36	0.78	1.8	3.9	7.6	14.4	29.1	48.5	108.9
cnrm_cm3	T63	1985	0.09	0.615	1.33	2.05	2.81	3.7	4.7	6.1	9.04	14.0	38.1
gfdl_cm2_1	$2.5^\circ \times 2^\circ$	1985	0.171	0.36	0.56	0.80	1.11	1.6	2.9	5.6	11.9	18.2	29.9
iap_fgoals1_0_g	T42	1985	0.239	0.50	0.79	1.15	1.68	2.5	3.7	5.5	8.6	11.6	19.7
inmcm3_0	$5^\circ \times 4^\circ$	1985	0.180	0.48	0.86	1.36	2.09	3.3	5.7	8.9	13.1	16.5	23.0
ipsl_cm4	$2.5^\circ \times 3.75^\circ$	1985	0.056	0.25	0.50	0.81	1.20	1.8	3.3	5.6	8.8	11.8	23.6
miroc3_2_hires	T106	1985	0.006	0.07	0.21	0.42	0.71	1.1	1.9	3.7	10.4	17.8	34.2
miroc3_2_medres	T42	1985	0.007	0.04	0.12	0.26	0.51	0.9	1.7	3.7	10.6	18.0	33.8
mpi_echam5	T63	1985	0.036	0.15	0.35	0.65	1.10	2.0	4.3	9.2	18.1	26.3	44.4
mri_cgcm2_3_2a	T42	1985	0.079	0.22	0.40	0.61	0.91	1.4	2.5	5.1	11.0	18.0	38.1
ukmo_hadgem1	$1.875^\circ \times 1.25^\circ$	1985	0.019	0.10	0.22	0.40	0.66	1.1	2.7	6.6	13.1	19.3	36.7
giss_e_r	$5^\circ \times 4^\circ$	1985	3.23	5.41	8.0	11.3	15.6	22.1	33.5	52.0	82.5	111.7	180.5
giss_e_r	$5^\circ \times 4^\circ$	1990	3.25	5.44	8.0	11.3	15.5	21.9	33.4	52.4	83.6	115.2	187.1
giss_e_r	$5^\circ \times 4^\circ$	1995	3.22	5.37	7.9	11.1	15.4	21.9	33.3	53.2	85.0	115.4	188.6
giss_e_r regrid	$2.5^\circ \times 2.5^\circ$	1985	4.39	6.91	9.8	13.4	18.2	25.6	37.2	53.3	78.4	102.3	156.8
giss_e_r regrid	$2.5^\circ \times 2.5^\circ$	1990	4.40	6.89	9.7	13.3	17.9	25.3	37.2	53.8	79.9	105.4	163.3
giss_e_r regrid	$2.5^\circ \times 2.5^\circ$	1995	4.39	6.87	9.7	13.2	18.0	25.5	37.4	54.5	80.8	105.6	164.0

5. Supporting Online Material: References

- S1. F. J. Wentz, L. Ricciardulli, K. Hilburn, C. Mears, *Science* **317**, 233 (2007).
- S2. G. A. Meehl, et al., *Bull. Amer. Met. Soc.* **88**, 1383 (2007).
- S3. E. M. Wilcox, L. J. Donner, *J. Climate* **20**, 53 (2007).
- S4. I. M. Held, B. J. Soden, *J. Climate* **19**, 5686 (2006).
- S5. M. R. Allen, W. J. Ingram, *Nature* **419**, 224 (2002).
- S6. G. Meehl, et al., Global climate projections, *Climate Change 2007: The Physical Science Basis. Contribution of Working Group I to the Fourth Assessment Report of the Inter-governmental Panel on Climate Change* (Cambridge University Press, Cambridge, United Kingdom and New York, NY, 2007), p. 757
- S7. R. P. Allan, *J. Geophys. Res.* **111**, D22105 (2006).
- S8. K. E. Trenberth, A. Dai, R. M. Rasmussen, D. B. Parsons, *Bull. Amer. Met. Soc.* **84**, 1205 (2003).